PCCP

Accepted Manuscript

This is an *Accepted Manuscript*, which has been through the Royal Society of Chemistry peer review process and has been accepted for publication.

Accepted Manuscripts are published online shortly after acceptance, before technical editing, formatting and proof reading. Using this free service, authors can make their results available to the community, in citable form, before we publish the edited article. We will replace this *Accepted Manuscript* with the edited and formatted *Advance Article* as soon as it is available.

You can find more information about *Accepted Manuscripts* in the **Information for Authors**.

Please note that technical editing may introduce minor changes to the text and/or graphics, which may alter content. The journal's standard **Terms & Conditions** and the **Ethical guidelines** still apply. In no event shall the Royal Society of Chemistry be held responsible for any errors or omissions in this *Accepted Manuscript* or any consequences arising from the use of any information it contains.

Physical Chemistry Chemical Physics

Journal Name

ARTICLE

Eu^{2+} Luminescence in Strontium Aluminates

D. Dutczak^{a,b}, T. Jüstel^a, C. Ronda^c and A. Meijerink^b

The luminescence properties of Eu^{2+} doped strontium aluminates are reported and reviewed for a variety of aluminates, viz. SrAl$_{12}$O$_{19}$, SrAl$_4$O$_7$, Sr$_4$Al$_{14}$O$_{25}$, SrAl$_2$O$_4$ and Sr$_3$Al$_2$O$_6$. The aim of the research is to investigate the role of local coordination and covalency of the aluminate host lattice, related to the Sr/Al ratio, on the optical properties of the Eu^{2+} ion. The UV and VUV excited luminescence spectra as well as luminescence decay curves were recorded to characterize the luminescence properties of the investigated aluminates. The emission of Eu^{2+} ions varies over a wide spectral range, from ultraviolet (UV) to red, for the series of aluminates. The variation in emission color can be related to the crystal-field splitting of the 5d levels and the covalent interaction with the surrounding oxygen anions. In the least covalent material, viz. SrAl$_{12}$O$_{19}$:Eu^{2+}, narrow line emission due to the ^{6}P$_{7/2}$ - ^{8}S$_{7/2}$ transition occurs at 4 K, indicating that the 4f^{6}5d excited state is situated above the ^{6}P$_{7/2}$ (4f^7) excited state around 360 nm. The most alkaline material, viz. Sr$_3$Al$_2$O$_6$:Eu^{2+} is the most covalent host and exhibits several d-f emission bands in the yellow to red spectral range due to the Eu^{2+} ions located on different crystallographic Sr^{2+} sites. The Eu^{2+} emission spectra in the other aluminates confirm the trend that with increasing Sr/Al ratio the Eu^{2+} emission shifts to longer wavelengths. Interesting differences are observed for the Eu^{2+} from different crystallographic sites which cannot always be related with apparent differences in the first oxygen coordination sphere. The discussion gives insight into how in a similar class of materials, strontium aluminates, the emission color of Eu^{2+} can be tuned over a wide spectral region.

1. Introduction

In recent years the luminescence of Eu^{2+} doped into strontium aluminates has received increasing attention due to the potential applications in fluorescent lamps, plasma display panels, light emitting diodes and persistent luminescent materials [1-5]. Strontium aluminates occur in several stoichiometries, for example: SrAl$_{12}$O$_{19}$, SrAl$_4$O$_7$, Sr$_4$Al$_{14}$O$_{25}$, SrAl$_2$O$_4$ and Sr$_3$Al$_2$O$_6$, arranged according to an increasing molar ratio of SrO to Al$_2$O$_3$ [6,7]. Divalent europium doped strontium aluminates usually show strong broad band luminescence due to transitions between the lowest excited [Xe]4f^{6}5d^1 configuration of the Eu^{2+} ion and the ^{8}S$_{7/2}$ ([Xe]4f^7) ground state [8-10]. The interaction of the 4f orbitals with their surrounding ions is weak, while the 5d orbitals are exposed to the surroundings and therefore the 4f^7 - 4f^{6}5d^1 transitions are strongly influenced by the chemical environment of Eu^{2+}. As a result, the emission of divalent europium can vary from ultraviolet to red, depending on the host lattice [11-13]. The shift is attributed to differences in the covalency in the chemical bonds between Eu^{2+} and the anion ligands, resulting in a shift of the center of gravity (also called the barycenter) of the 5d-orbitals (centroid shift) and the crystal field splitting of the 5d orbitals of Eu^{2+} [8,14]. For the presently studied strontium

aluminates, the covalency and the crystal field are affected by the Sr/Al ratio. Based on ionization potential arguments, the covalency increases with decreasing Al content (or increasing alkalinity) in the series of Sr-aluminates. The second factor, the crystal field splitting is determined by the number of ligands surrounding the central ion, their distance, their charge, and the coordination geometry [15]. In compounds with a high coordination number the distances between the central ion and the ligands are large and thus the strength of the crystal field is low. Additionally, crystal field splitting tends to be large for an octahedral environment and decreases with increasing coordination number. In case of the strontium aluminates, the Sr coordination number decreases with decreasing Al content. Both factors are expected to contribute to a red shift of the Eu^{2+} emission on decreasing the Al content in the strontium aluminates

^{a} Department of Chemical Engineering, Münster University of Applied Sciences, Stegerwaldstr. 39, D-48565 Steinfurt, Germany.

^{b} CMI, Debye Institute for Nanomaterials Science, Utrecht University, P.O. Box 80 000, 3508 TA Utrecht, The Netherlands.

^{c} Philips Group Innovation - Eindhoven, High Tech Campus 4, 5656 AE Eindhoven, The Netherlands.

In this paper, the luminescence properties of various Eu^{2+} doped strontium aluminates, viz. $SrAl_{12}O_{19}$, $SrAl_4O_7$, $Sr_4Al_{14}O_{25}$, $SrAl_2O_4$, and $Sr_3Al_2O_6$ will be discussed on the basis of their covalent character and the crystal field splitting of the d-orbitals of Eu^{2+} in these compounds. Moreover, the band gap energy and the position of the 5d levels of Eu^{2+} in these strontium aluminates were studied with UV-VUV synchrotron radiation. The results will be discussed in relation to previous research on the Eu^{2+} luminescence in strontium aluminates. In addition to providing insights in the trends and origin for the large variation in emission color for these aluminates, new results and insights will be provided for the luminescence properties for Eu^{2+} on the various crystallographic sites in different aluminates based on concentration and temperature dependent luminescence excitation and emission spectra and time resolved luminescence.

2. Experimental

2.1 Synthesis

Synthesis of $SrAl_{12}O_{19}$, $Sr_4Al_{14}O_{25}$, $SrAl_2O_4$, $Sr_3Al_2O_6$ by a solid state method

Strontium carbonate (Dr. Paul Lohmann), aluminum oxide (Degussa), and europium oxide (Treibacher), were weighed and ground with acetone. Small quantities of boric acid were used as a flux. The mixed powders were first precalcined at 1000 ^{o}C in air. The second calcination step was performed in a reducing atmosphere of 90% N_2 and 10% H_2 at the following temperatures: 1300 ^{o}C ($SrAl_{12}O_{19}$), 1400 ^{o}C ($Sr_4Al_{14}O_{25}$), 1350 ^{o}C ($SrAl_2O_4$). In case of $Sr_3Al_2O_6$ the second calcination step was performed in a reducing atmosphere of 30% N_2 and 70% H_2 at 1300 ^{o}C, to prevent (partial) oxidation to Eu^{3+}, giving rise to the characteristic red Eu^{3+} line emission. Concentrations of Eu^{2+}, typically 0.1%, 0.5% or 1%, are all mole percent relative to Sr^{2+}.

Synthesis of $SrAl_4O_7$ by the citric acid method

Citric acid (VWR Prolabo), ethylene glycol, aluminum nitrate nonahydrate (VWR Prolabo), and strontium carbonate (Dr. Paul Lohmann), were used as the starting materials. Citric acid was dissolved in ethylene glycol, followed by the addition of aluminum nitrate nonahydrate. After achieving complete dissolution a stoichiometric amount of strontium carbonate was added to the solution. During the process, the pH was maintained at 3 by addition of 25% ammonia solution. The obtained viscous mass was dried at 140 ^{o}C for 4 hours and then calcined at 800 ^{o}C in air. The powder was finally heated at 1050 ^{o}C in reducing atmosphere of 90% N_2 and 10% H_2. This method was chosen because the first method did not result in phase pure $SrAl_4O_7$.

2.2. Characterization

The X-ray powder diffraction measurements were performed on Rigaku MiniFlex II, operated in the Bragg–

Brentano geometry and equipped with a Cu-anode X-ray source. The XRD patterns of the obtained samples matched the following references: $SrAl_{12}O_{19}$ (ICSD #2006), $SrAl_4O_7$ (ICSD #2817), $Sr_4Al_{14}O_{25}$ (ICSD #88527), $SrAl_2O_4$ (ICSD #26466) and $Sr_3Al_2O_6$ (ICSD #71860). X-ray absorption near-edge structure (XANES) spectroscopic measurements at the Eu LIII edge were performed at beamline 20BM (PNC/XSD) at the Advanced Photon Source (APS).

In the Supporting Information the XRD patterns are shown together with the reference patterns (Figure S1). The excellent agreement between the recorded and reference patterns indicate that all materials are single phase. To investigate the valence state of the Eu also XANES measurements were performed on two of the aluminates ($SrAl_2O_4$:Eu0.1% and $Sr_4Al_{14}O_{25}$:Eu0.1%). The XANES spectra (Figure S2, Supporting Information) confirm that Eu is in the divalent state.

The room temperature emission and excitation spectra were measured with a fluorescence spectrometer FLS920 (Edinburgh Instruments) equipped with a 450 W Xenon discharge lamp, monochromator TMS300 (Czerny-Tuner configuration), operated in the single photon counting mode using a R2658P (Hamamatsu) photo-multiplier tube. The emission and excitation spectra at liquid helium temperature were recorded on an Edinburgh spectrofluorometer equipped with an Oxford Instruments liquid helium flow cryostat for measurements down to 4 K.

The high resolution vacuum ultraviolet (VUV) spectroscopy measurements were carried out at the SUPERLUMI station of HASYLAB (DESY, Germany), using synchrotron radiation from the DORIS III storage ring as excitation source. The experimental set-up was equipped with a 2 m McPherson primary monochromator with resolution of ~0.1 nm. Emission was recorded using an ARC Spectra Pro-308i monochromator equipped with a Hamamatsu R6358P photomultiplier [16]. The samples were mounted on the cold finger of a liquid He flow cryostat. The excitation spectra were corrected for the wavelength-dependent intensity variation using the excitation spectrum of sodium salicylate as a reference, assuming that the quantum efficiency of sodium salicylate is excitation wavelength independent.

Luminescence life time measurements were performed using a FLS920 fluorescence spectrometer (Edinburgh Instruments) equipped with a TMS300 monochromator (Czerny-Tuner), operated in the single photon counting mode using a R2658P (Hamamatsu) photomultiplier tube. As excitation source a pulsed LASER Diode EPL-(375 nm) and a pulsed LED EPLED-(265 nm) were used. Decay time measurements were also performed using an Excimer laser (Lambda Physik) pulsed dye laser (10 ns pulses) in combination with a 1 GHz digital oscilloscope (Tektronix).

3. Results and discussion

3.1 SrAl$_{12}$O$_{19}$:Eu^{2+}

Strontium hexaaluminate has a very low SrO/Al$_2$O$_3$ ratio (1/6) and is the most ionic compound among all investigated strontium aluminates. The SrAl$_{12}$O$_{19}$ host crystallizes in the hexagonal space group P6$_3$/mmc [17,18]. The structure is derived from magnetoplumbite and consists of two spinel blocks containing Al^{3+} cations separated by intermediate mirror planes containing Al^{3+} and Sr^{2+} cations (Figure 1a) [19-22]. The Sr^{2+} ions are located in a symmetric coordination of 12 oxygen anions. The average Sr-O distance is large, 2.77 Å (Figure 1b). In this structure type only one crystallographic site
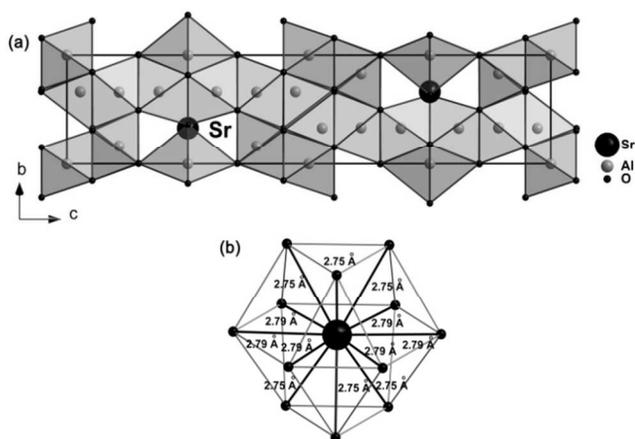
Figure 1 (a) Unit cell of SrAl$_{12}$O$_{19}$ along the a - axis, (b) Local coordination geometry of Sr^{2+}.

for strontium exists. Eu^{2+} ions substitute for Sr^{2+} ions because of the similar atomic radius and the same charge. The 12-fold coordinated Sr site in the magnetoplumbite structure experiences a weak crystal field. The low degree of covalent character of the Eu-O bond and the weak crystal field are expected to result in a rather high energy of the 5d - 4f transition of Eu^{2+}.

The excitation spectra of the Eu^{2+} emission in SrAl$_{12}$O$_{19}$:1% Eu^{2+} at 4 and 300 K are presented in Figure 2. The room temperature excitation spectrum for 397 nm emission shows a broad band ranging from 200 to 370 nm which is attributed to the electric-dipole allowed transition from the ^{8}S$_{7/2}$ 4f^7 ground state to the 4f^{6}5d^1 excited states of Eu^{2+}. In addition to the transition of Eu^{2+}, a sharp edge at ca. 160 nm is observed. This is assigned to the fundamental absorption edge excitation corresponding to the energy between the top of the valence band and the bottom of the conduction band i.e. the band gap energy [23]. The band gap energy of SrAl$_{12}$O$_{19}$:Eu^{2+} estimated from the half height value of the intensity of the absorption

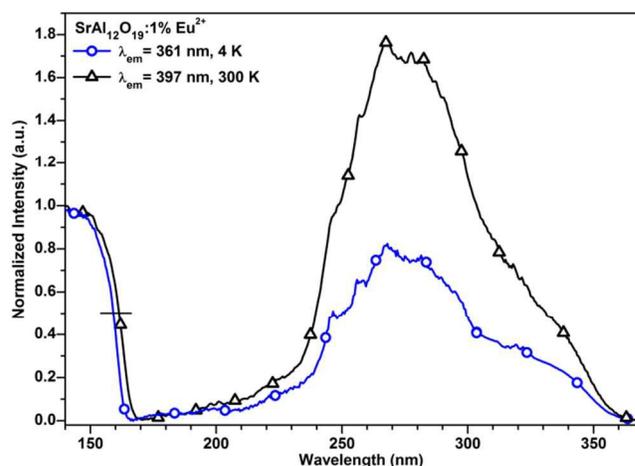**Figure 2 Excitation spectra of SrAl$_{12}$O$_{19}$:1%Eu^{2+} at 4 K recorded for 361 nm emission and at 300 K recorded 397 nm emisison.**

band edge is equal to 7.76 eV. The shape of the excitation spectrum of SrAl$_{12}$O$_{19}$:1% Eu^{2+} for the 397 nm emission band does not change significantly with temperature. There is small shift to lower energies of the absorption edge between 4 and 300 K.

The emission spectrum however, changes drastically with temperature. The emission spectrum at 300 K (see Figure 3) is dominated by 4f^{6}5d^1 → 4f^7 broad band emission peaking at 397 nm [13,24]. Around 360 nm some weak sharp lines can be observed on top of the broad band. Upon cooling to 4 K the broad band emission decreases in intensity while the narrow line emission increases. At 4 K only line emission is observed. The narrow emission lines are ascribed to the intraconfigurational 4f^7 transitions ^{6}P$_{7/2}$ - ^{8}S$_{7/2}$ [25-27]. The ^{6}P$_{7/2}$ emission can be observed because the lowest 4f^{6}5d level of Eu^{2+} is located at higher energy than the ^{6}P$_{7/2}$ level [8,28-30] as
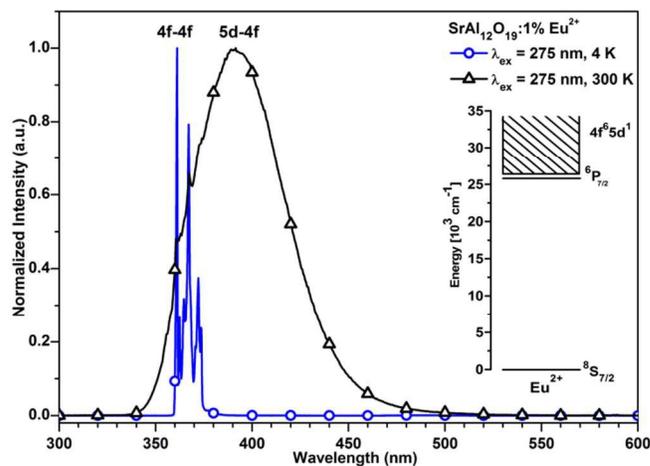

Figure 3 Emission spectra of SrAl$_{12}$O$_{19}$:1%Eu^{2+} at 4 K and 300 K recorded at 275 nm excitation. The inset presents the simplified energy level scheme of Eu^{2+} in SrAl$_{12}$O$_{19}$.

shown by the simplified energy level scheme of Eu^{2+} in $SrAl_{12}O_{19}$ inserted in Figure 3. At room temperature, the emission from the $^6P_{7/2}$ level is weak due to the small energy difference between the lowest $4f^65d$ level and the $^6P_{7/2}$ level. The $4f^65d$ level is thermally populated at 300 K and in view of the much higher radiative decay rate of the allowed d-f transition, this emission dominates at room temperature. The observation of line emission for Eu^{2+} in the $SrAl_{12}O_{19}$ host is a consequence of the small crystal field splitting of the $4f^65d^1$ configuration of Eu^{2+} on the Sr^{2+} site (due to the high coordination number 12) and the small centroid shift (due to the ionic nature of the host lattice for the very low SrO/Al_2O_3 ratio) [8]. The onset of the f-d excitation band (see Figure 2) is consistent with a position of the lowest $4f^65d$ state around 360 nm, just above the $^6P_{7/2}$ levels.

In Figure 4 the temperature dependence of the relative intensities of the $4f^65d$ emission and the $^6P_{7/2}$ 4f - 4f emission are plotted. The cross-over from 4f-4f emission to d-f emission occurs between 100 and 200 K. As the $4f^65d$ level is thermally populated, the fast parity allowed emission from this state takes over as is typically observed for Eu^{2+} in host lattices where the $4f^65d$ is situated just above the $^6P_{7/2}$ state. The integrated emission intensity is constant up to 350 K. Above 350 K temperature quenching sets in and the quenching temperature of the d-f emission is 380 K. The quenching temperature is defined as the temperature at which the emission intensity is reduced to 50% of the initial intensity.
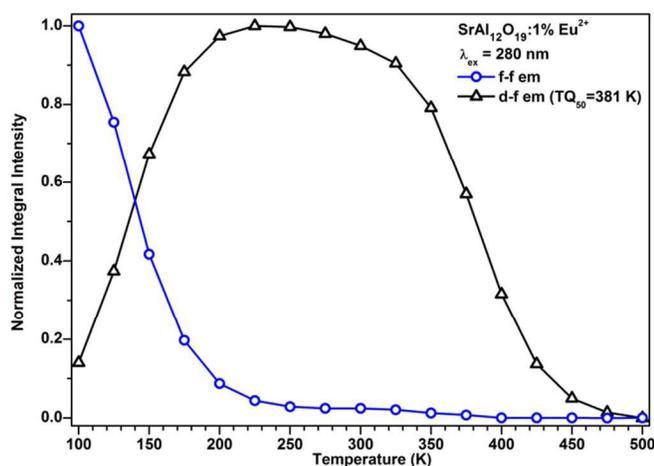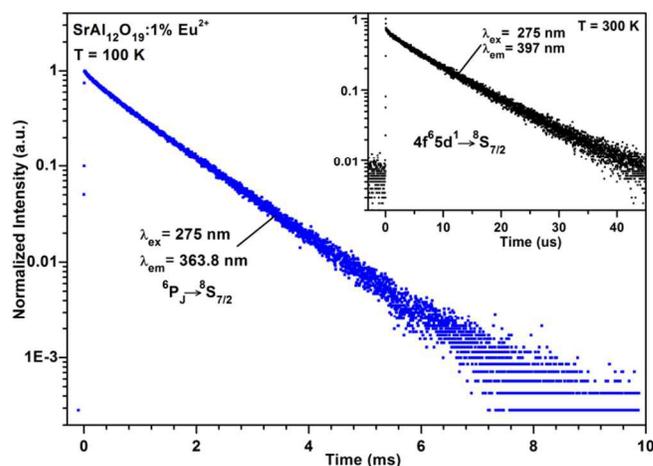

Figure 5 Decay curve of the emission band originating from the ^6P_J - $^8S_{7/2}$ transition at 100 K. The inset shows the decay curve of the $4f^65d^1$ - $^8S_{7/2}$ emission at 300 K.

The decay time of the $4f^65d^1$-$^8S_{7/2}$ transition in $SrAl_{12}O_{19}$:1%Eu^{2+} measured at 300 K is equal to 8.0 μs, about 8 times longer than the expected radiative decay rate. Based on the decay time at 300 K and the temperature dependence of the $^6P_{7/2}$ and $4f^65d$ emission (Figure 4), the energy difference between the two levels can be estimated to be 400 cm^{-1}. This number is consistent with an energy difference of 0.046 eV (371 cm^{-1}) determined from the decrease of the $^6P_{7/2}$ emission intensity with temperature [30].

3.2 $SrAl_4O_7$:Eu^{2+}

The compound strontium dialuminate crystallizes in a monoclinic structure with the space group C12/c1 [7]. The $SrAl_4O_7$ lattice consists of corner sharing AlO_4 tetrahedral layers and strontium ions, which are embedded in between the layers [31,32]. In this structure only one crystallographic site for strontium exists. The strontium ions have seven nearest neighbor oxygen ions at variable distances. The average Sr-O distance is 2.61 Å (Figure 6).
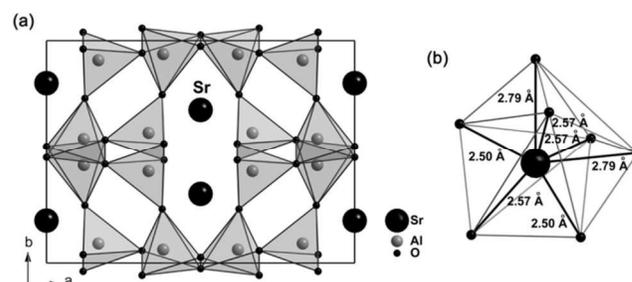

Figure 4 The emission intensity dependence on temperature for the f-f and d-f emission in $SrAl_{12}O_{19}$:1%Eu^{2+}.

The decay curves of the Eu^{2+} emission in $SrAl_{12}O_{19}$:1%Eu^{2+} were measured at 100 and 300 K (Figure 5). The decay curves are single-exponential. At 100 K the lifetime of the Eu^{2+} emission is largely determined by the intraconfigurational ^6P_J -$^8S_{7/2}$ transition and is 0.9 ms. At 300 K, the $^6P_{7/2}$ and $4f^65d^1$ levels are both populated and in thermal equilibrium, therefore the decay time of $SrAl_{12}O_{19}$:1%Eu^{2+} measured at this temperature is much longer than radiative decay of 5d - 4f emission of Eu^{2+} which is in 1 μs range.

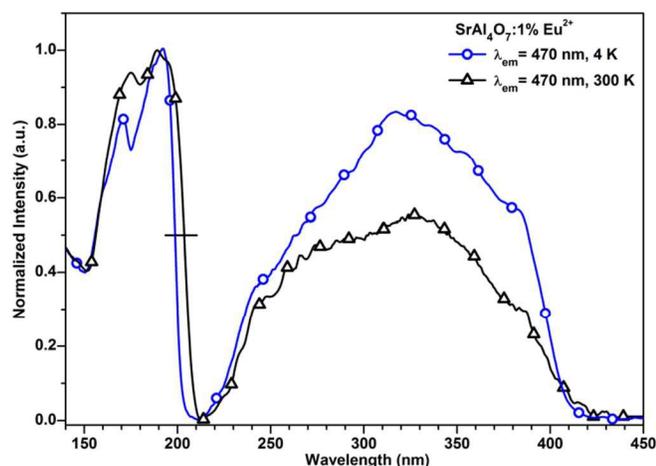**Figure 6 (a) Unit cell of $SrAl_4O_7$ along the c - axis, (b) Local coordination geometry environment of Sr^{2+}.**

Figure 7 Excitation spectra of SrAl$_4$O$_7$:1%Eu^{2+} at 4 K and 300 K recorded at 470 nm.

In Figure 7 the excitation spectra of the Eu^{2+} emission in SrAl$_4$O$_7$:1% Eu^{2+} at 10 and 300 K are shown. The excitation spectra consist of two broad bands. The band with a sharp edge around 200 nm in the VUV region is due to the absorption of the host lattice and the second broad band in the UV region, between 220 and 400 nm is assigned to the 4f^7→ 4f^{6}5d absorption transitions of the Eu^{2+} ions. The band gap energy of SrAl$_4$O$_7$:1% Eu^{2+} estimated from the absorption edge is equal to 6.3 eV at 4 K and 6.1 eV at room temperature. The shift to lower energies of the band gap with increasing temperature is commonly observed, also for semiconductors and is ascribed to thermal expansion of the host lattice [33].

The emission spectra of SrAl$_4$O$_7$:1%Eu^{2+} at 4 and 300 K are shown in Figure 8. The maximum of the emission is around 470 nm. The emission corresponds to the allowed electric-dipole transition 4f^{6}5d → 4f^7 of Eu^{2+}. The SrAl$_4$O$_7$:Eu^{2+} phosphor emits at longer wavelength [34-36] in comparison to the more ionic SrAl$_{12}$O$_{19}$:Eu^{2+}.

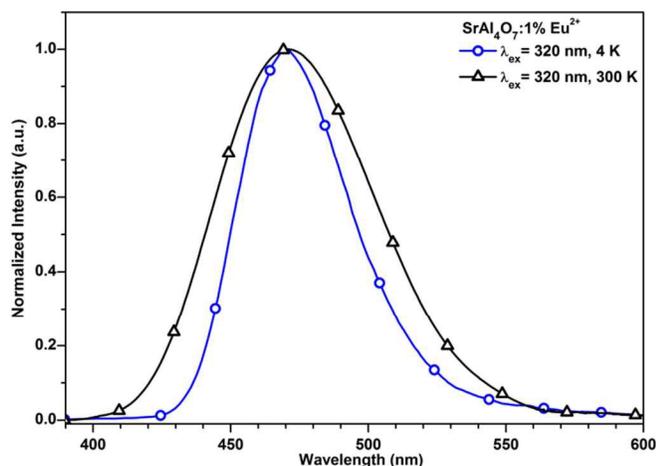**Figure 8 Emission spectra of SrAl$_4$O$_7$:1%Eu^{2+} at 4 K and 300 K recorded at 320 nm excitation.**

A significant increase of the full width at half maximum (FWHM) of the emission band can be observed with increasing temperature. The broadening of the peak with increasing temperature is caused by the rising population of higher vibrational levels at higher temperatures and is commonly observed for Eu^{2+} emission.

In Figure 9 the temperature dependence of the emission is shown. Already below room temperature there is strong quenching of the emission. The onset of temperature quenching is at 150 and at 260 K the intensity has dropped to half the initial value.
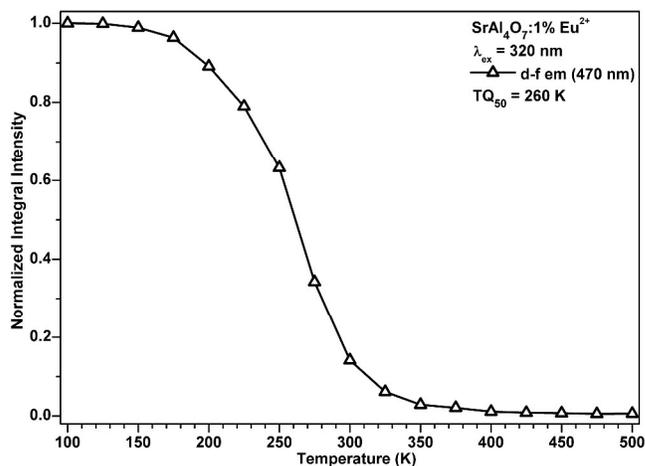

Figure 9 The emission intensity dependence on the temperature for SrAl$_4$O$_7$:1%Eu^{2+}.

3.3 Sr$_4$Al$_{14}$O$_{25}$:Eu^{2+}

The next investigated member of the strontium aluminate family is Sr$_4$Al$_{14}$O$_{25}$ which has a SrO/Al$_2$O$_3$ ratio of 4/7. The Sr$_4$Al$_{14}$O$_{25}$ host crystallizes in an orthorhombic crystal system with space group Pmma [37]. As shown in the projection of Sr$_4$Al$_{14}$O$_{25}$ along the crystal plane (Figure 10), the structure consists of two layers made up of AlO$_6$ octahedra separated by double layer of AlO$_4$ tetrahedra [38-40]. The structural data reveal two different strontium sites with coordination numbers 10 and 7 in the Sr$_4$Al$_{14}$O$_{25}$. Because of the similar ionic radius, Eu^{2+} ions replace Sr^{2+} ions leading to two different types of luminescent Eu^{2+} centers. The average Sr-O bond length for 10-fold coordinated strontium is equal to 2.77 Å and is longer than for the 7-fold coordinated strontium (2.62 Å) [37,41]. The interactions between oxygen and strontium ions at the 10-fold coordinated site will be weaker than for the 7-fold coordinated site. A higher covalency and larger crystal field splitting are expected for Eu^{2+} in the 7-fold coordinated site than in the 10-fold site due to the shorter Sr-O distances.
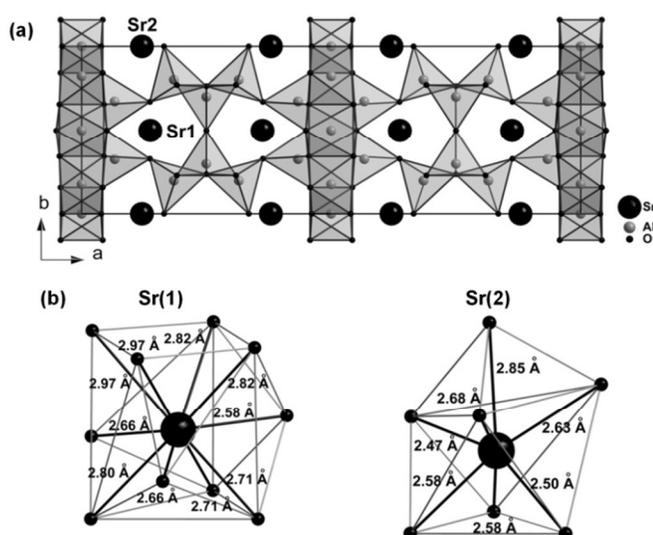
Figure 10 (a) Unit cell of $Sr_4Al_{14}O_{25}$ along the c - axis, (b) Local coordination geometry environment of nonequivalent Sr^{2+} sites.

The UV excited luminescence spectra of $Sr_4Al_{14}O_{25}$:1%Eu^{2+} at room temperature and at 4 K are presented in Figure 11. The emission spectra change with temperature. At low temperature, the Eu^{2+} emission from both sites is clearly observed. The spectrum consists of two bands peaking at 425 and 490 nm [42]. We assign the high energy emission peak to Eu^{2+} on the 10-fold coordinated site and the low energy peak to Eu^{2+} with 7-fold coordination in line with the smaller crystal field splitting for the 10-coordinated site. One can notice, that the Eu^{2+} emission from the 10-fold coordinated site of $Sr_4Al_{14}O_{25}$:1%Eu^{2+} (425 nm) lies in between the Eu^{2+} emission peaks from the 12 coordinated site in $SrAl_{12}O_{19}$:1%Eu^{2+} (397 nm) and the 7-fold coordinated site in $SrAl_4O_7$:1%Eu^{2+} (470 nm). The Eu^{2+} emission from the 7-fold coordinated site in $Sr_4Al_{14}O_{25}$:1%Eu^{2+} (490 nm) is observed at longer wavelength than that of the 7-fold coordinated site in $SrAl_2O_4$:1%Eu^{2+} (470 nm).
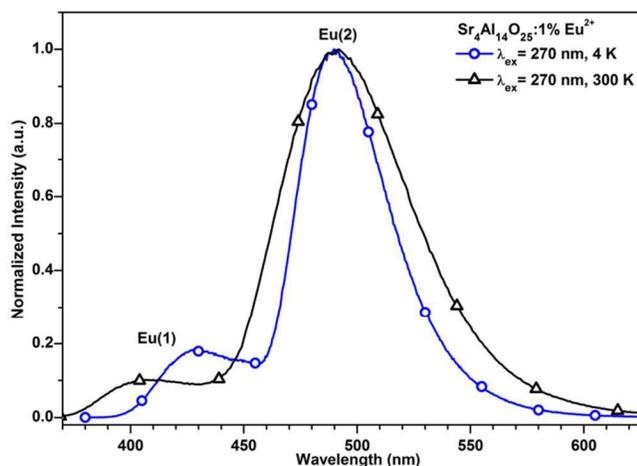

Figure 11 Emission spectra of $Sr_4Al_{14}O_{25}$:1%Eu^{2+} at 4 K and 300 K recorded at 270 nm excitation.

This is in line with the higher covalency in $Sr_4Al_{14}O_{25}$:1%Eu^{2+}. At room temperature energy transfer between Eu^{2+} ions on the two sites occurs and the intensity of the high energy emission band is reduced in comparison to the spectrum recorded at 4 K. The more efficient energy transfer at 300 K is attributed to an increase of the spectral overlap between the high energy emission band and the excitation band of the emission band peaking at 490 nm with increasing temperature, due to thermal broadening of the bands. The larger spectral overlap is further enhanced by a large spectral shift of the high energy emission from 425 to 400 nm between 4 and 300 K. Consequently, emission from $Eu(1)$ can be transferred to the $Eu(2)$ center, which leads to a decrease in the short wavelength emission intensity and an intensity enhancement in the long wavelength emission [42-45]. Energy transfer between different Eu^{2+} sites can be confirmed by emission spectra of $Sr_4Al_{14}O_{25}$ with lower Eu^{2+} concentration (Figure 12).
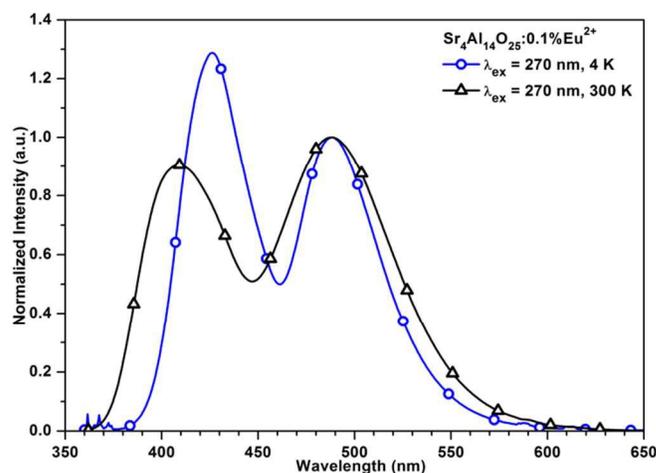

Figure 12 Emission spectra of $Sr_4Al_{14}O_{25}$:0.1%Eu^{2+} at 4 K and 300 K recorded at 270 nm.

The probability of energy transfer among Eu^{2+} ions increases with increasing Eu^{2+} concentration. For an Eu^{2+} concentration of 1 mole%, the intensity of the high energy emission measured at 4 K is weak (Figure 11). As the concentration is decreased to 0.1% the two emission bands have similar intensities (Figure 12) [37].

The temperature dependence of the relative intensities of the two emission bands is plotted in Figure 13. The quenching temperature for the emission is 410 K.

The spectra in Figures 11 and 12 show an interesting effect of temperature on the position of the emission bands. The position of the low energy band is almost temperature independent, as is usually observed, while the position of the high energy band shifts to shorter wavelengths with increasing temperature. Around 200 K a sudden shift from 425 nm to 400 nm is observed. The origin of the shift was discussed by the authors elsewhere [46]. The emission at 400 and 490 nm were assigned to 'normal' *d-f* emission from Eu^{2+} on the 10- and 7 coordinated sites, respectively, while the 425 nm emission was assigned to 'anomalous' Eu^{2+} trapped exciton emission (ETE). The temperature induced shift was explained by a transition from anomalous Eu^{2+} trapped exciton emission to normal $4f^65d$ emission
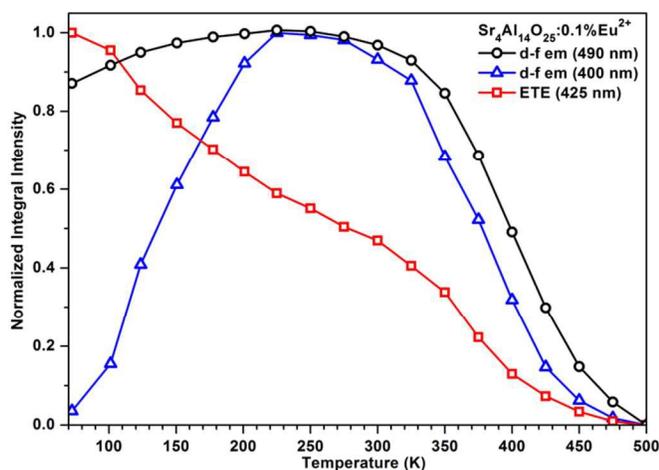
Figure 13 The emission intensity dependence on the temperature of $Sr_4Al_{14}O_{25}$:0.1%Eu^{2+} for different emission bands.

due to the position of the $4f^65d$ state just above the ETE state but below the conduction band.

The excitation spectra of $Sr_4Al_{14}O_{25}$:0.1%Eu^{2+} recorded for the two types of emission centers are shown in Figure 14 and demonstrate different shapes and positions of the maxima. The spectrum recorded for the Eu(2) center consists of a structured band between 220 to 400 nm with a maximum at 280 nm while the excitation spectrum recorded for the Eu(1) center has a broader band ranging from 210 to 460 nm. The excitation spectrum does not change strongly with temperature. As was mentioned before, the broad excitation band of the Eu(2) center overlaps with the emission spectrum of Eu(1), causing energy transfer from Eu^{2+} ions emitting at higher energy to Eu^{2+} ions emitting at lower energies. In addition to the direct excitation of the Eu^{2+} ion via the $4f^7 \rightarrow 4f^65d^1$ bands the excitation band in VUV, with an onset at 200 nm and an inflection point at ~195 nm (6.3 eV) in the excitation spectrum of $Sr_4Al_{14}O_{25}$:1%Eu^{2+} is interpreted as the host lattice excitation.

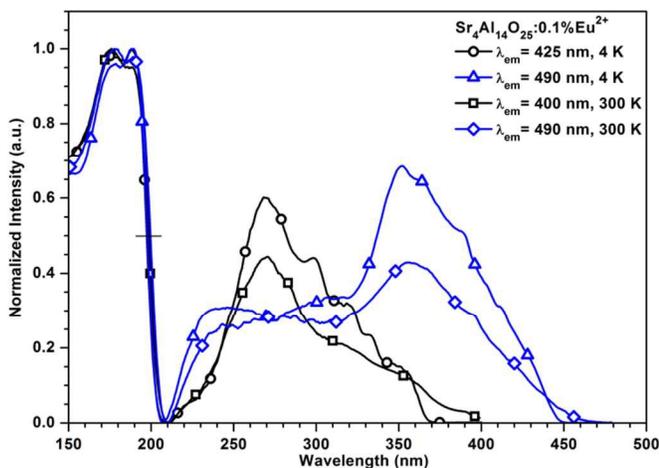**Figure 14 UV and VUV excitation spectra of $Sr_4Al_{14}O_{25}$:0.1%Eu^{2+} recorded at 420 nm (at 4 K), 400 nm (at 300 K) and 490 nm (at 4 K and 300 K) emission.**

Based on this, the bandgap of $Sr_4Al_{14}O_{25}$ is determined to be 6.3 eV.

Decay curves of the Eu^{2+} emission in $Sr_4Al_{14}O_{25}$:0.1%Eu^{2+} were recorded at different emission wavelengths for the Eu(1) center and Eu(2) centre (Figure 15). The decay times of the two different emissions are in the µs range (see Table 1) but differ significantly, which confirms that these emission bands originate from Eu^{2+} ions located in different sites in the crystal. It is well known that the lifetime of d-f emission of Eu^{2+} is usually around 1 µs [47]. From the decay time at 490 nm (0.9 µs) and using the λ^3 dependence of the decay time of allowed transitions [48] we calculate a decay time of 0.57 µs for the emission at 425 nm (both at 4 K), in good agreement with the observed value of 0.6 µs. At 300 K, only the decay time of the emission at shorter wavelengths changes significantly, which can be due to energy transfer from Eu(1) ions to Eu(2) ions (also making the decay curve slightly non-exponential) and also to partial temperature quenching of the emission at 300 K. The occurrence of energy transfer is consistent with the change in the excitation spectrum for the 490 nm emission. At 300 K the relative intensity in the high energy part of the spectrum, between 250 and 350 nm, is higher than at 4 K. In this spectral area there is overlap with the excitation spectrum of the Eu(1) and energy transfer from Eu(1) to Eu(2) can explain the observed increase in relative intensity.
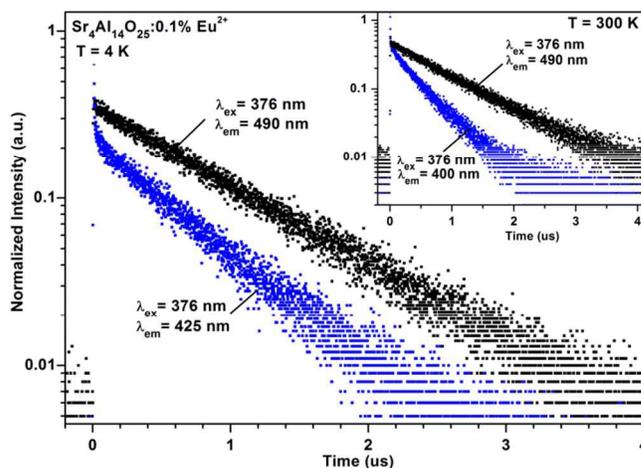

Figure 15 Decay curve of $Sr_4Al_{14}O_{25}$:0.1%Eu^{2+} at 4 K at emission wavelengths indicated in the figure. The inset shows decay curve of $Sr_4Al_{14}O_{25}$:0.1%Eu^{2+} at 300 K.

Table 1 Decay times of different Eu^{2+} centres in $Sr_4Al_{14}O_{25}$:0.1%Eu^{2+} derived from fits to single exponential decay of the decay curves in Figure 15.

Emission band [nm]	Decay time at 4 K [µs]	Decay time at 300 K [µs]
425 / 400	0.6	0.3
490	0.9	0.9

3.4. $SrAl_2O_4:Eu^{2+}$

The $SrAl_2O_4$ host crystallizes in the stuffed tridymite type of structure with space group P21 [49]. The structure consists of rings formed by six corner sharing AlO_4 tetrahedra (Figure 16).

The strontium ions are situated within the channels formed by the AlO_4 tetrahedra [50]. In the $SrAl_2O_4$ host, there are two nonequivalent strontium sites with the same coordination number and similar average Sr-O distances. The sites differ only by a slight distortion of their square planes [51]. Both strontium sites in the lattice have nine adjacent oxygen ions. The distances of two oxygen ions are relatively large, therefore coordination number 7 or 7+2 can be considered [52]. The average distances for these 7 oxygen ions are 2.69 Å and 2.67 Å for Sr1 and Sr2, respectively. Due to the similar local environments (based on the coordination number) of Eu^{2+} ions substituting different Sr^{2+} ions, the Eu^{2+} centers are expected to show similar luminescence properties. Different emission bands have been reported for Eu^{2+} at the two different Sr-sites in $SrAl_2O_4$, in spite of the similarity in coordination, at 450 and 520 nm [53].
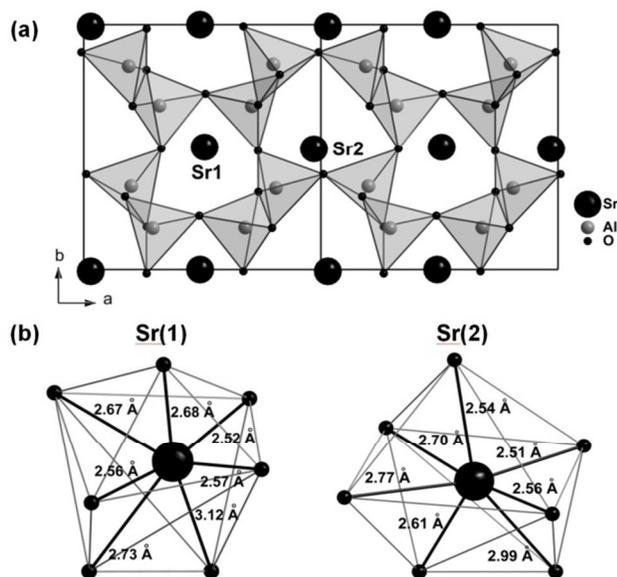

Figure 16 (a) Unit cell of $SrAl_2O_4$ along the c - axis, (b) Local coordination geometry environment of Sr^{2+}.

The excitation spectra recorded at 4 K for the two emission bands consist of broad bands due to the interconfigurational $4f^7$ - $4f^65d^1$ transitions of Eu^{2+} between 200 and 410 nm for the short wavelength emission and between 200 and 460 nm for the long wavelength emission band (Figure 17).
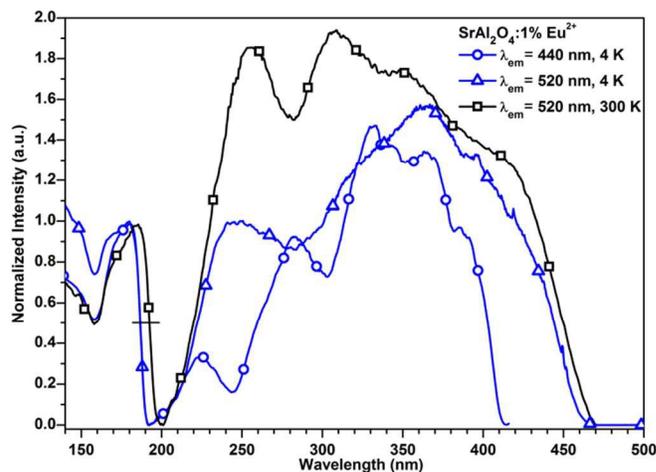

Figure 17 VUV and UV excitation spectra of $SrAl_2O_4:1\%Eu^{2+}$ recorded at 440 nm (at 4 K) and 520 nm (at 4 K and 300 K).

In addition, the excitation of Eu^{2+} can occur via the host lattice. From the position of the absorption edge at 188 nm a band gap energy value of 6.6 eV for room temperature is determined and is in good agreement with a previous study [52]. At 4 K the edge shifts to slightly higher energies. The host lattice absorption edge is at the same position for both emissions confirming that both types of Eu^{2+} ions are incorporated in the same lattice and that the second emission band does not originate from Eu^{2+} in impurity phases.

The emission spectra of $SrAl_2O_4:1\%$ Eu^{2+} recorded under 350 nm excitation at 300 and 4 K temperature are presented in Figure 18. The spectra of $SrAl_2O_4:1\%$ Eu^{2+} change with temperature. At room temperature only one asymmetric emission band is observed [54-58] while at 4 K an additional band at 445 nm appears, consistent with observations in the literature [59, 60].

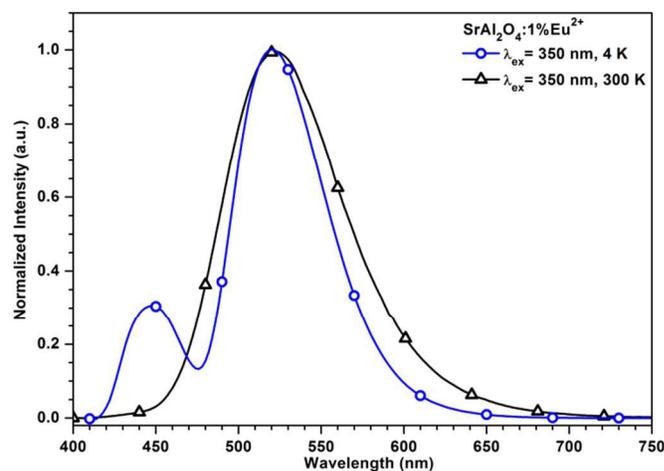**Figure 18 Emission spectra of $SrAl_2O_4:1\%Eu^{2+}$ at 4 and 300 K recorded under 350 nm excitation.**

In Figure 19 the temperature dependence of the emission bands is depicted. The 520 nm emission starts to quench above 350 K and has a quenching temperature of 440 K. The 445 nm
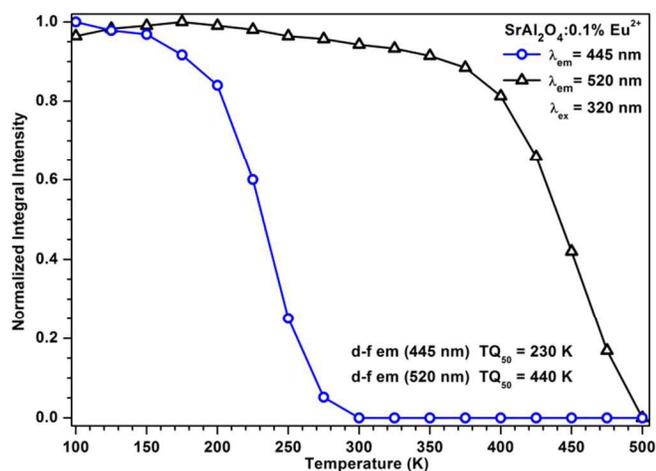
Figure 19 Emission intensity dependence on the temperature of SrAl$_2$O$_4$:0.1%Eu^{2+} for the emission band at 445 and 520 nm.

emission band is quenched at much lower temperatures and is characterized by a quenching temperature of 230 K. The fact that this emission is fully quenched at 300 K explains why the emission is not observed in the 300 K emission spectrum.

The origin of the high energy emission band is controversial in the literature. Some authors assigned the 445 and 520 nm emission bands to emission of the Eu^{2+} ion located at two nonequivalent strontium sites in the SrAl$_2$O$_4$ host [53,61]. However, the two strontium sites in the SrAl$_2$O$_4$ are very similar and differ only by a slight distortion of their square planes [51]. The similar coordination for both sites is expected to give rise similar luminescence properties due to comparable crystal field strengths and centroid shifts.

Poort et al. [53] explained the large energy difference between two emission bands by the differences in the orientation of the d-orbitals in linear chains of Sr-ions along the a-axis. The larger distances to the neighboring oxygen ions in the linear chains of Sr-ions for the one site will lead to preferential orientation of the d-orbital, thus lowering the energy of the d-state and leading to lower energy (520 nm) emission.

However several researchers rejected the hypothesis that the 445 and 520 nm emission bands originate from Eu^{2+} in two strontium sites and offered alternative explanations. Clabau et al. [51] proposed that the 445 nm emission arises from the charge transfer from oxygen to residual Eu^{3+} that takes place upon UV irradiation and is associated with hole trapping at Sr^{2+} vacancies. A different explanation was given by Hölsä et al. [62] suggesting that 445 nm emission originates from a higher Eu^{2+} 4f^{6}5d^1 state.

More recently, Botterman at al. [61] reported a detailed investigation on the origin of both emission bands in SrAl$_2$O$_4$:Eu. On the basis of the structure of the excitation spectra for both emission bands and crystallographic information it was argued that the 445 nm and 520 nm emission bands originate from Eu^{2+} ions substituting for the two different Sr sites in SrAl$_2$O$_4$. In spite of the similarity in oxygen coordination, differences in bond lengths (average and effective) to the oxygen ligands exist for the two sites and the

difference in geometry was used to explain the difference in emission and excitation spectra and to assign the redshifted 520 nm emission band to the Sr(1) site.

The lifetime measurements of both emissions bands performed in this studies (Figure 20), support the postulate that the 445 nm and 520 nm emission bands originate from Eu^{2+} ions substituting for the two different Sr sites.
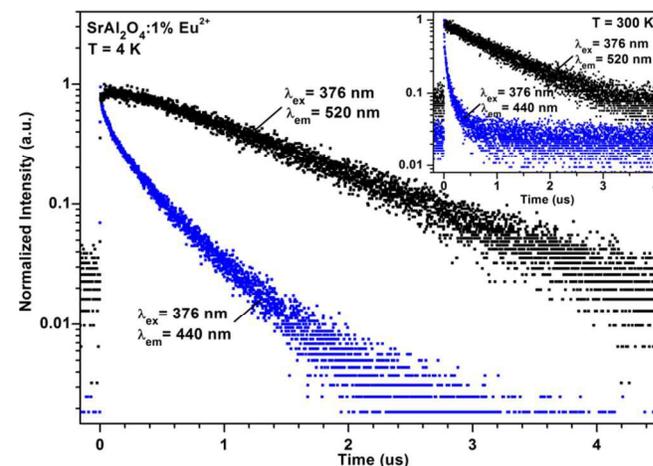

Figure 20 Decay curves of Eu^{2+} emission in SrAl$_2$O$_4$:1%Eu^{2+} at 4 K for emission wavelengths indicated in the Figure. The inset shows decay curves of SrAl$_2$O$_4$:0.1%Eu^{2+} at 300 K.

The measured µs lifetime of the emission at 445 nm is consistent with the expected lifetime of the Eu^{2+} emission. Also, charge transfer emission has never been observed for Eu^{3+}, nor has emission from higher 4f^{6}5d states been observed for Eu^{2+} due to the multitude of closely spaced 4f^{6}5d states giving rise to fast relaxation to the lowest 4f^{6}5d state. Finally, concentration dependent measurements support the explanation that the two bands originate from the two different crystallographic sites in the SrAl$_2$O$_4$ host. For 1% Eu^{2+} the intensity of the higher energy band is weak (see Figure 20) while for a sample with 0.1% Eu^{2+} both bands have similar intensity (see Ref. [53]). This is typically observed for energy transfer between two different crystallographic Eu-sites (see also Figures 11 and 12).

Decay curves for the emission bands of SrAl$_2$O$_4$:1%Eu^{2+} were recorded at different emission energies assigned to the Eu(1) and Eu(2) centres. The obtained decay times are collected in Table 2.

Table 2 Decay times of the emission for the different Eu^{2+} centres in SrAl$_2$O$_4$:1%Eu^{2+}

Emission band [nm]	Decay time at 4 K [µs]	Decay time at 300 K [µs]
445	0.4	-
520	1.2	0.7

The average decay time of the 445 nm emission is 0.4 µs and is shorter than the decay time of 520 nm emission of 1.2 µs [59]. The decay time of the 520 nm emission is consistent with the

expected decay time for 520 nm emission [48]. The λ^3 dependence of the decay time yields a value of about 0.8 μs for the 445 nm emission. The shorter decay time observed, 0.4 μs, indicates that energy transfer takes place, shortening the decay time. This explanation is supported by the low relative intensity of the 445 nm emission band and the non-exponential character of the decay curve.

3.5. $Sr_3Al_2O_6$:Eu^{2+}

Due to the very high Sr/Al ratio (3/1), the $Sr_3Al_2O_6$ host is the most covalent and alkaline phosphor among all aluminates investigated here. The $Sr_3Al_2O_6$ host is related to the superstructures of perovskites and crystallizes with the space group Pa3 [63]. According to the structural data, six different strontium sites exist in $Sr_3Al_2O_6$ (Figure 21).

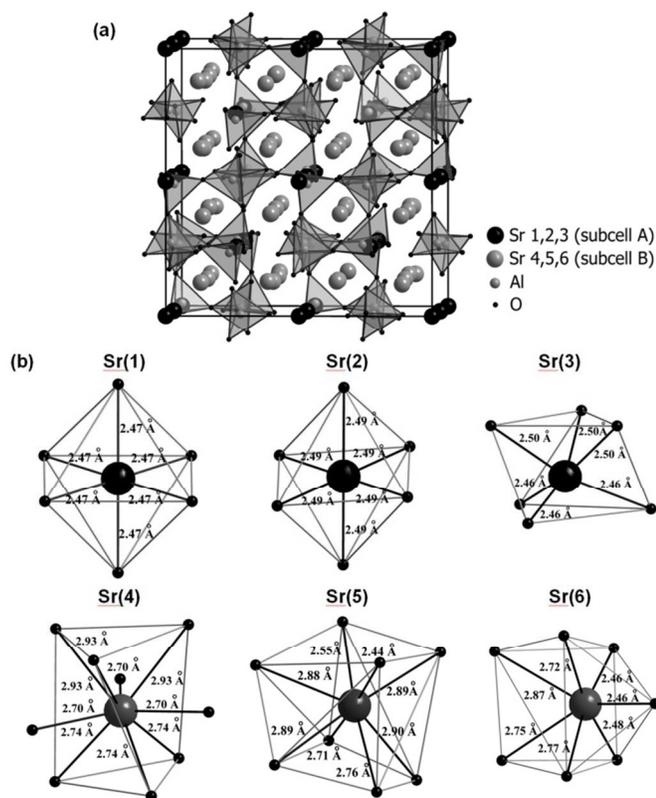**Figure 21 (a) Unit cell of $Sr_3Al_2O_6$ (b) Local coordination geometry environment of nonequivalent Sr^{2+} sites.**

Three of them Sr(1), Sr(2), Sr(3) form subcell (A), and Sr(4), Sr(5), Sr(6) form subcell (B). The strontium atoms from subcell (A) form a three-dimensional cubic matrix in the $Sr_3Al_2O_6$ host, while the strontium atoms from subcell (B) are situated within the channels formed by subcell (A) [63]. All strontium atoms in framework (A) are coordinated to six oxygen atoms. The sites differ only by distortion of their square planes. The polyhedron around Sr(1) and Sr(2) is described as a distorted octahedron, while polyhedron around Sr(3) as distorted trigonal prism. The average Sr-O bond length is equal to 2.47 Å, 2.49 Å, 2.48 Å for Sr(1), Sr(2) and Sr(3), respectively. Strontium atoms forming framework (B) occupy rather

irregular environments and the average Sr-O distances in framework (B) are longer than for framework (A). Sr(4) atoms coordinated by nine oxygen atoms have an average Sr-O distance equal to 2.79 Å, while Sr(5) atoms coordinated by 8 have an average Sr-O distance 2.75 Å. Sr(6) atoms are coordinated by seven oxygen atoms with an average Sr-O distance 2.64 Å. The interactions between the oxygen and strontium ions forming sublattice (A) are stronger than for sublattice (B), in view of the shorter Sr-O distances. One can assume (based on co-ordination numbers) that the covalence and crystal field effects are stronger for Sr(1), Sr(2), Sr(3) sites than for the Sr(4), Sr(5), Sr(6) sites.

During last few years, a number of publications have appeared on the luminescence properties of Eu^{2+} in $Sr_3Al_2O_6$. The reported results concerning the position of Eu^{2+} emission in $Sr_3Al_2O_6$:1%Eu^{2+} are confusing or even in contradiction to each other. Some authors [64-67] have reported green emission of $Sr_3Al_2O_6$: Eu^{2+} peaking around 510 nm, under 360 nm excitation. Yu et al. [68] and Shin et al. [69] have also reported broad green band emission but peaking at 518 and 522, respectively.

Zhang [70-72] and Yuesheng [73] have reported red Eu^{2+} emission at 612 nm under 473 nm excitation, while Huang [74] and Zhou [75] reported emission at 618 nm in the same material. Additionally, emission at 405 and 435 nm from $Sr_3Al_2O_6$:Eu^{2+} have been reported [76]. The contradictory results for $Sr_3Al_2O_6$:Eu^{2+} were explained in 2011 by Huang [77] showing that all the previous reports were mostly correct. The observed differences in emission spectra of $Sr_3Al_2O_6$:Eu^{2+} are caused by differences in excitation wavelengths. The green and the red emissions originate from different crystallographic sites for Eu^{2+}. The $Sr_3Al_2O_6$:Eu^{2+}/Dy^{3+} phosphor emits a yellow–green light upon UV illumination, and a bright red light upon visible light illumination. Similar results have been reported by Zhan et al.in 2011 [78].

Figure 22 shows the emission spectra of $Sr_3Al_2O_6$:Eu^{2+} under 377 and 467 nm excitation at 4 K. The $Sr_3Al_2O_6$:Eu^{2+} phosphor shows green emission peaking at 538 nm excited at 377 nm with an additional broad band at longer wavelength. Under lower energy excitation the red emission centered at 625 nm can be observed. Clearly, multiple emission bands/colors can be observed depending on the excitation wavelength. According to structural data, six different strontium sites exist in $Sr_3Al_2O_6$. Therefore, one can expect that substitution of Sr^{2+} sites by Eu^{2+} ions should lead to six different types of luminescent Eu^{2+} centers. Three strontium sites have the same coordination number 6 and similar coordination geometry thus the emission bands from these sites are expected to show significant overlap. Based on the low coordination number (6) and short distances to the surrounding oxygens, the emission for Eu^{2+} on these sites is expected at the longest wavelengths and to form the band centered at 625 nm. Note that some fine structure is observed at the onset of the 625 nm emission band with a sharp zero-phonon like line at 585 nm. The green emission can be assigned to an emission center formed in sites with higher coordination numbers (9, 8, 7). By changing the excitation wavelength, emission from different sites can be selective enhanced. Under excitation at 377 nm green emission coming from sites coordinated by 9, 8, 7 oxygen ions, as well as red emission originating from sites coordinated by 6 oxygen ions are visible. Under long wavelength excitation green
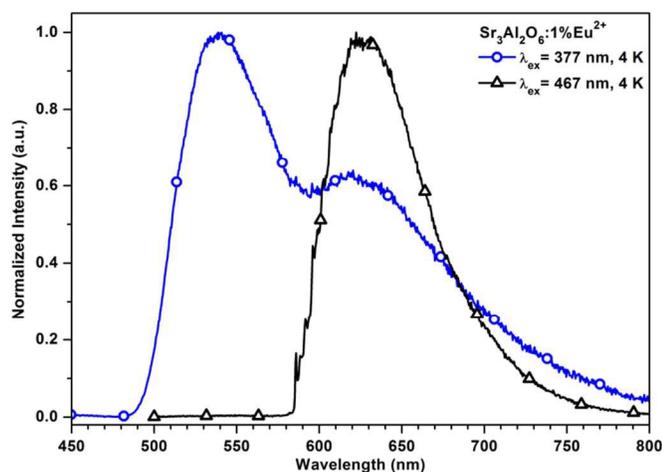
Figure 22 Emission spectra of $Sr_3Al_2O_6$:1%Eu^{2+} at 4 K recorded for 377 and 467 nm excitation.

emission is not visible anymore while the red emission becomes dominant. Only broad band emission centered at 625 nm is visible under 467 nm excitation.

The temperature dependence of the emission intensity for the green and red emission is depicted in Figure 23. Both the green and red emissions are characterized by low quenching temperatures and are not observable at room temperature. The low energy red emission of $Sr_3Al_2O_6$:1%Eu^{2+} is almost completely quenched already at 100 K, while the quenching temperature for high energy emission is higher; the green emission is quenched completely at 200 K. There are different explanations for the low quenching temperatures. The quenching may be caused by thermally induced photoionization. However, a low quenching temperature is often observed for long wavelength emission from Eu^{2+}.
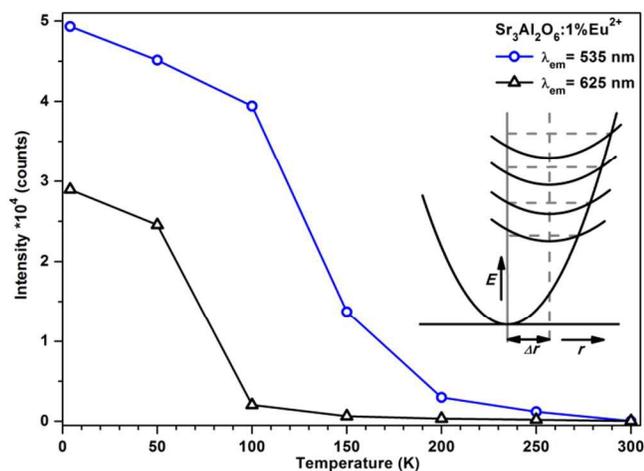

Figure 23 The emission intensity dependence on the temperature of $Sr_3Al_2O_6$:1%Eu^{2+}. Inset presents the configurational coordinate diagrams for the same off-set and different excited state energies to illustrate the relation between quenching temperature and energy of emission bands.

To explain the quenching a configurational coordinate diagram as presented in the inset in Figure 23 can be considered. The activation energy for thermally activated cross-over from the excited state to the ground state becomes smaller when the energy of the excited state is lower for the same Stokes shift. In case of low energy emission for the same off-set of the parabola (relaxation in the excited state), the quenching temperature is lower. This makes it difficult to prepare efficient red d-f emitting phosphors with a large Stokes shift. However, one can also not exclude thermal quenching by thermally activated photoionization of an electron from the $4f^65d$ state to the conduction band.

The excitation spectra of $Sr_3Al_2O_6$:1%Eu^{2+} varies for different emission maxima (Figure 24). The excitation spectrum recorded at 625 nm shows a broad band ranging from 240 to 575 nm while excitation spectrum recorded at shorter wavelengths shows a broad band ranging from 260 to 450 nm. The band between 260 and 450 nm for 538 nm emission is assigned to $4f^7$ - $4f^65d$ excitation bands for the sites with higher coordination numbers while the broad band between 250 and 570 nm contains contribution from $4f^7$ - $4f^65d$ excitation bands of all sites, due to partial energy transfer from the high energy sites to the red emitting Eu^{2+} ions.
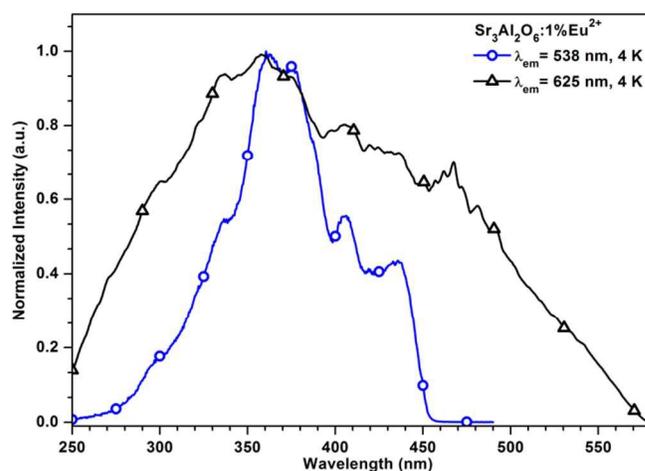

Figure 24 Excitation spectra of $Sr_3Al_2O_6$:1%Eu^{2+} at 4 K recorded for different emission wavelengths. The lines around 470 nm arise from Xe-lamp lines due to imperfect correction of the spectrum for variations in the lamp intensity as a function of wavelength.

The different emission bands also show different luminescence decay times (Figure 25). At 4 K the decay curve of higher energy emission is strongly multi-exponential, due to the energy transfer to the Eu^{2+}-sites emitting at lower energy and possibly also due to overlapping emission bands from different sites with different Eu^{2+} emission decay times. The decay curve of the lower energy emission is also not single-exponential, because of energy transfer between three six coordinated sites and differences in decay time for overlapping emission bands. Based on the present experiments, the conflicting reports in the literature on the emission color of the Eu^{2+} emission in $Sr_3Al_2O_6$:1%Eu^{2+} can be understood. Two groups of sites can be distinguished. Sites with higher coordination numbers

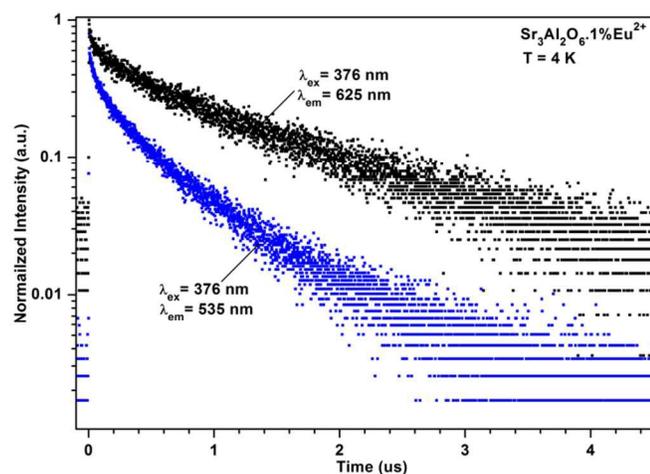**Figure 25 Decay curves of Eu^{2+} emission in Sr$_3$Al$_2$O$_6$:1%Eu^{2+} at 4 K under pulsed 376 nm excitation for 535 and 625 nm emission.**

Figure 26 Emission spectra of Eu^{2+} in different strontium aluminates measured at 300 K (Emission spectrum of Sr$_3$Al$_2$O$_6$:1%Eu^{2+} was measured at 4 K due to strong thermal quenching).

and larger Sr-O distances gives rise to green d-f emission of Eu^{2+} while the three slightly different sites with a six-coordination of oxygen give rise to red emission due to the high degree of covalency and large crystal field splitting, but only at low temperatures. At higher temperatures (above 100 K) the red emission is quenched and only green emission is observed. At room temperature the emission is quenched for both sites

General discussion and conclusions

The luminescence properties of Eu^{2+} have been investigated and reviewed for a series of strontium aluminates including SrAl$_{12}$O$_{19}$, SrAl$_4$O$_7$, Sr$_4$Al$_{14}$O$_{25}$, SrAl$_2$O$_4$ and Sr$_3$Al$_2$O$_6$. In this series of aluminates the SrO/Al$_2$O$_3$ ratio changes from 1/6 to 3/1. The systematic studies have shown that the changes in Sr/Al ratio strongly affected the position of the 4f^{6}5d^1 - 4f^7 emission of Eu^{2+}. The changes are explained by covalency effects (higher energy of the barycenter of the 4f^{6}5d states in the more ionic Al$_2$O$_3$ rich hosts) and changes in the local coordination, where in the Al$_2$O$_3$-rich compositions lower coordination numbers are encountered, leading to larger crystal field splitting. Both effects contribute to a shift of the lowest 4f^{6}5d component, from which the Eu^{2+} emission originates, to lower energies. The effect is illustrated in Figure 26 where the Eu^{2+} emission spectra for the five different compositions are collected. The emission of Eu^{2+} in the investigated aluminates varies from near UV to the red spectral range in the order expected based on the SrO/Al$_2$O$_3$ ratio. The most ionic compounds: SrAl$_{12}$O$_{19}$:Eu^{2+}, with the lowest SrO/Al$_2$O$_3$ ratio (1/6) among all strontium aluminates emits in near UV spectral range (398 nm). On increasing the Sr/Al ratio, a red shift of the emission of Eu^{2+} is obtained. The most alkaline material, viz. Sr$_3$Al$_2$O$_6$:Eu^{2+}, exhibits several emission bands among which the longest wavelength emission peaks at 625 nm. Usually a shift from the UV to the visible is achieved by changes in the nature of the ligands.
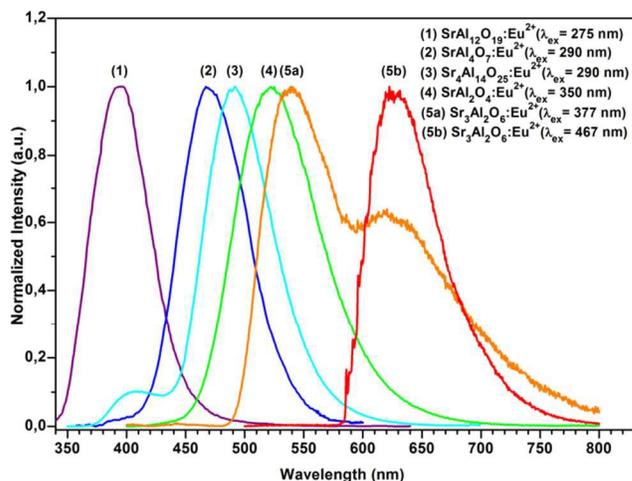
High energy UV emission is commonly observed in fluoride hosts while long wavelength red emission can be realized by incorporating Eu^{2+} ions in hosts with highly covalent anions, e.g. nitrides and sulfides. Here the full spectrum is covered in a single type of host, Sr-aluminates.

In Table 3 characteristic luminescence properties are collected for the Eu^{2+} emission for the different crystallographic sites in the five aluminates investigated. In addition to the host band gap and emission maxima, the bandwidth (FWHM) of the emission bands at 4 and 300 K, the luminescence quenching temperature (defined as the temperature at which the emission intensity is reduced to half the low temperature value) and luminescence decay times are included for the various sites with different coordination. The bandwidths are included as a measure of the electron-phonon coupling. Commonly, the Stokes shift is used to characterize the phonon-coupling strength. For Eu^{2+} it is notoriously difficult to determine the Stokes shift since it is hard to identify the position of the excitation maximum for the transition to the emitting 4f^6(^{7}F$_0$)5d state on the increasing background of the higher energy 4f^6(^{7}F$_J$)5d states. The 4f^6(^{7}F$_J$)5d states give rise to a ~6000-7000 cm^{-1} wide excitation band with a continuously increasing intensity, in which the position of the 4f^6(^{7}F$_0$)5d excitation band cannot be identified. The general trend of shifting the Eu^{2+} emission to lower energies for increasing SrO content is clearly observed in Table 3. As was mentioned before, not only covalency has an influence on the position of the Eu^{2+} emission band. The spectral position of the Eu^{2+} emission in strontium aluminates is a combined effect of covalency and the crystal field strength. The influence of the crystal field on the position of Eu^{2+} emission is especially visible in the aluminates with more than one strontium sites: Sr$_4$Al$_{14}$O$_{25}$:Eu^{2+}, SrAl$_2$O$_4$:Eu^{2+} and Sr$_3$Al$_2$O$_6$:Eu^{2+}. Lower coordination numbers result in a shift to lower energies, consistent with the larger crystal field splitting expected for lower coordination numbers. However, surprisingly large differences in emission wavelengths are observed for Eu^{2+} on the two similar crystallographic sites in SrAl$_2$O$_4$. To explain the difference more

subtle interactions and also Stokes shift effects are considered, demonstrating the sensitivity of the d-f emission wavelength for Eu^{2+} to the local surroundings.

Finally it is interesting to consider the luminescence quenching temperatures and the relation with the width of the emission bands. The values for TQ_{50} vary strongly and are consistent with values reported in the literature for $SrAl_{12}O_{19}$ and $SrAl_2O_4:Eu^{2+}$ [10]. For thermal quenching through thermally activated cross-over from the excited state to the ground state, a clear correlation with the Stokes shift and the width of the emission band are expected. A larger off-set between ground state and excited state lowers the quenching temperature and leads to a larger Stokes shift and a larger bandwidth. Because it is difficult to accurately determine the Stokes shift for the

Eu^{2+} emission, here we use the width of the emission band as a more reliable parameter for the electron-phonon coupling. Also, lower quenching temperatures are expected for longer wavelength emission (see also Figure 23). Clearly, neither correlation is observed. The quenching temperature varies between 70 and 440 K while the emission bandwidths are remarkable similar (~2000 cm^{-1} at 4 K and ~3000 cm^{-1} at 300 K). The longest wavelength emission does show the lowest quenching temperature, but there is no clear correlation between emission wavelength and TQ_{50}. Based on these observations it seems that thermally induced photoionization is the dominant mechanism for temperature quenching of the Eu^{2+} emission in this series of aluminates, similar to many other compositions [10].

Table 3 The band gap energies, coordination numbers, main emission peak positions, 4 and 300 K full width half maximum of emission bands (FWHM), quenching temperature (T_Q) and luminescence decay times for the Eu^{2+} emission from different Sr-sites in strontium aluminates

	$SrAl_{12}O_{19}:Eu^{2+}$	$SrAl_4O_7:Eu^{2+}$	$Sr_4Al_{14}O_{25}:Eu^{2+}$		$SrAl_2O_4:Eu^{2+}$		$Sr_3Al_2O_6:Eu^{2+}$	
SrO/Al_2O_3	1/6	1/2	4/7		1/1		1/3	
Band gap at 4 K (eV)	7.8	6.3	6.3		6.6		6.2	
Coordination number	12	7	10	7	7	7	9, 8, 7	6, 6, 6
Emission max at 4 K (nm)	f-f (397 at 300 K)	470	425 (ETE) 400 at 300 K	490	445	520	535	625
FWHM at 4 K (cm^{-1})	-	2100	2300	2200	1950	2300	-	1500
FWHM at 300 K (cm^{-1})	3600	3000	3100	2900	-	3000	-	-
Thermal quenching TQ_{50} (K)	380	260	380 (400 nm)	410	230	440	130	70
Decay time at 4 K (µs)	8.0 (at 300 K)	-	0.6	0.9	0.4	1.2	0.6	1.1

Conclusions

In conclusion, the luminescence of Eu^{2+} has been studied in a series of strontium aluminates, viz. $SrAl_{12}O_{19}$, $SrAl_4O_7$, $Sr_4Al_{14}O_{25}$, $SrAl_2O_4$ and $Sr_3Al_2O_6$. The strong variation of the emission color from ultraviolet (UV) to red is explained based on covalency (increasing for higher SrO content) and crystal field splitting (higher for lower coordination numbers) and gives rise to a continuous shift of the Eu^{2+} emission to longer wavelengths upon increasing the SrO/Al_2O_3 ratio. The luminescence properties (emission life times, quenching temperature, and bandwidth) for Eu^{2+} on the different crystallographic sites in the $Sr_4Al_{14}O_{25}$ and $SrAl_2O_4$ show a clear correlation between life time and emission wavelength, generally following the expected λ^3 dependence. The quenching temperatures vary strongly, independent of the remarkably similar luminescence bandwidths, and do not show a clear correlation with composition.

Acknowledgement

References

[1]   C. Feldmann, T. Jüstel, C.R. Ronda, P.J. Schmidt, *Advanced Functional Materials*, 2003, **13**, 511

[2]   A.M. Srivastava, H. S. Nalwa (Ed.), *Handbook of Luminescence, Display Materials and Devices*, American Scientific Publishers, 2003

[3]   C. R. Ronda (Ed.), *Luminescence: from theory to applications*, Wiley-VCH, Weinheim, 2008.

[4]   J. Hölsä, *Electrochemical Society Interface,* 2009, **18**, 42

[5]   M. Born, T. Jüstel, *Chemie unserer Zeit*, 2006, **40**, 294

[6]   X. Ye, W. Zhuang, J. Wang, W. Yuan, Z. Qiao, *Journal of Phase Equilibria and Diffusion*, 2007, **28**, 362

[7]   M. Capron, A. Douy, *Journal of the American Ceramic Society*, 2002, **85**, 3036

[8]   G. Blasse, B.C. Grabmaier, *Luminescent Materials*, Springer, Berlin, 1994

[9]   P. Dorenbos, *Journal of Physics*: *Condensed Matter*, 2003, **15**, 575

[10] P. Dorenbos, *Journal of Physics*: *Condensed Matter*, 2003, **15,** 2645

[11] P. Dorenbos, *Journal of Luminescence*, 2003, **104**, 239

[12] K. Van den Eeckhout, P. F. Smet, D. Poelman, *Materials*, 2010, **3**, 2536

[13] D. Ravichandran, S. T. Johnson, S. Erdei, R. Roy, W. B. White, *Displays*, 1999, **19**, 197

[14] P. Dorenbos, J. Andriessen, C.W.E. van Eijk, *Journal of Solid State Chemistry*, 2003, **171**, 133

[15] P. Dorenbos, *Journal of Alloys and Compounds*, 2002, **341**, 156

[16] G. Zimmerer, *Nuclear Instruments and Methods in Physics Research Section A*, 1991, **308**, 178

[17] A. J. Lindop, C. Mathews, D.W. Goodwin, *Acta Crystallographica Section B*, 1975, **31**, 2940

[18] P.B. Braun, *Philips research reports*, 1957, **12**, 491

[19] Z. Nie, K. Lim, J. Zhang, X. Wang, *Journal of Luminescence*, 2009, **129**, 844

[20] K. Kimura, M. Ohgaki, K. Tanaka, H. Morikawa, F. Marumo, *Journal of Solid State Chemistry*, 1996, **87**, 186

[21] J.-G. Park, A. N. Cormack, *Korean Journal of Crystallography*, 2000, **11**, 173

[22] K. Harindranath, K. Anusree Viswanath, C. Vinod Chandran, T. Bräuniger, P.K. Madhu, T.G. Ajithkumar, P.A. Joy, *Solid State Communications*, 2010, **150**, 262

[23] P. Dorenbos, *Journal of Luminescence*, 2005, **111**, 8

[24] V.Singh, T.K. Gundu Rao, J.-J. Zhu, *Journal* of *Solid State Chemistry*, 2006, **179**, 2589

[25] G. Blasse, A. Bril, *Philips research reports,* 1968, **23**

[26] J.M.P.J. Verstegen, J.L. Sommerdijk and A. Bril, *Journal of Luminescence*, 1974, **9**, 420

[27] A. L. N. Stevels, A. D. M. Schrama-de Pauw, *Journal of Solid State Science and Technology*, 1976, **123**, 691

[28] A. Meijerink, *Journal of Luminescence*, 1993, **55**, 125

[29] A. Ellens, A. Meijerink, G. Blasse, *Journal of Luminescence*, 1994, **59**, 293

[30] T. Katsumata, Y. Kohno, H. Kubo, S. Komuro, T. Morikawa, *Rev. Sci. Instr.,* 2005, **76**, 084901

[31] R. Jagannathan, R. P. Rao, T. R. N. Kutty, *Materials Research Bulletin*, 1992, **27**, 459

[32] M. Karmaoui , M-G Willinger, L. Mafra, T. Herntrich, N. Pinna, *Nanoscale*, 2009, **1**, 360

[33] T. Toyodat, M. Tomita, S. Hanba, *Journal of Semiconductor Technology and Science*, 1986, **1**, 295

[34] K. R. S. Preethi, C-H. Lu, J. Thirumalai, R. Jagannathan, T. S. Natarajan, N. U. Nayak, I. Radhakrishna, M. Jayachandran, D. C. Trivedi, *Journal* of *Physics D*: *Applied Physics*, 2004, **37**, 2664

[35] T. Katsumata, K. Sasajima, T. Nabae, S. Komuro, T. Morikawa, *Journal of the American Ceramic Society* 1998, **81**, 413

[36] M.G. Eskin, H. Kurt, M. A.Gulgun, C.W. Ow-Yang, *MRS Proceedings,* 2011, **1309**, 28

[37] Q. Li, J. Zhao, F. Sun, *Journal of Rare Earth*, 2010, **28**, 26

[38] Z. Wu, J. Shi, J. Wang, M. Gong, Q. Su, *Journal of Materials Science: Materials in Electronics*, 2008, **19**, 339

[39] C. Zhao, D. Chen, Y. Yuan, M. Wu, *Materials Science and Engineering: B,* 2006, **133**, 20

[40] M. Capron, F. Fayon, D. Massiot, A. Douy, *Chemistry of Materials,* 2003, **15**, 575

[39] D. Wang, M. Wang G. L. Lu, *Journal of Materials Science*, 1999, **34**, 4959

[42] E. Nakazawa, Y. Murazaki, S. Saito, *Journal of Applied Physics*, 2006, **100**, 113113-1

[43] Y. Lin, Z. Tang, Z. Zhang, C. W. Nan, *Applied Physics Letters*, 2002, **81**, 996

[44] M. Peng, Z. Pei, G. Hong, Q. Su, *Chemical Physics Letters*, 2003, **371**, 1

[45] N. Thompson, P. Murugaraj, C. Rix, D. E. Mainwaring, *Journal of Alloys and Compounds*, 2012, **537**, 147

[46] D. Dutczak, C. Ronda, T. Jüstel, A.Meijerink, *The Journal of Physical Chemistry A,* 2014, **118**, 1617

[47] G. Blasse, W. L. Wanmaker, J. W. Tervrugt, A. Bril, *Philips research reports*, 1968, **23**, 189

[48] S.H.M. Poort, A. Meijerink, G. Blasse, *Journal of Physics and Chemistry of Solids*, 1997, **58**, 1451

[49] A.-R. Schulze, H. K. Müller-Buschbaum, *European Journal of Inorganic Chemistry*, 1981, **475**, 205

[50] A. K. Prodjosantoso, B. J. Kennedy, *Journal of Solid State Chemistry*, 2002, **168**, 229

[51] F. Clabau, X. Rocquefelte, S. Jobic, P. Deniard, M.-H. Whangbo, A. Garcia, T. Le Mercier, *Chemistry of Materials*, 2005, **17**, 3904

[52] J. Hölsä, T. Laamanen, M. Lastusaari, J. Niittykoski, P. Novák, *Journal of Rare Earth*, 2009, **27**, 550

[53] S. H. M. Poort, W. P. Blokpoel, G. Blasse, *Chemistry of Materials*, 1995, **7**, 1547

[54] T. Matsuzawa, Y. Aoki, N. Takeuchi, Y. Murayama, *Journal of Electrochemical Society*, 1996, **143**, 2670

[55] Z. Qiu, Y. Zhou, M. Lu, A. Zhang, Q. Ma, *Acta Materialia*, 2007, **55**, 2615

[56] T. Ishigaki, H. Mizushina, K. Uematsu, N. Matsushita, M. Yoshimura, K. Toda, M. Sato, *Materials Science and Engineering: B*, 2010, **173**, 109

[57] T. Aitasalo, P. Deren, J. Hölsä, H. Jungren, J.-C. Krupa, M. Lastusaari, J. Legendziewicz, J. Niittykoski, W. Stręk, *Journal of Solid State Chemistry*, 2003, **171**, 114

[58] J. Niittykoski, T. Aitasalo, J. Hölsä, H. Jungner, M. Lastusaari, M. Parkkinen, M. Tukia, *Journal of Alloys and Compounds*, 2004, **374**, 108

[59] T. Aitasalo, J. Hölsä, H. Jungner, J.-C. Krupa, M. Lastusaari, J. Legendziewicz, J. Niittykoski, *Radiation Measurements*, 2004, **38**, 727

[60] V. Chernov, T.M. Piters, R. Meléndrez, W.M. Yen, E. Cruz-Zaragoza, M. Barboza-Flores, *Radiation Measurements* , 2007, **42**, 668

[61] J. Botterman, J. J. Joos, P.F. Smet, *Physical Review B*, 2014, **90,** 085147

[62] J. Hölsä, T. Laamanen, M. Lastusaari, M. Malkamäki, P. Novák, *Highlights and Hasylab Annual Report*, 2009, **91**

[63] J. A. Alonso, I. Rasines, J. L. Soubeyroux, *Inorganic Chemistry*, 1990, **29**, 4768

[64] Ch. Chang, W. Li, X. Huang, Z. Wang, X. Chen, X. Qian, R. Guo, Y. Ding, D. Mao, *Journal of Luminescence*, 2010, **130**, 347

[65] P. Mingying, D. Ning, Q. Yanbo, W. Baotao, W. Chen, Ch. Danping, Q. Jianrong, *Journal of Rare Earth*, 2006, **24**, 749

[66] M. Akiyama, C.-N. Xu, K. Nonuka, T. Watanabe, *Applied Physics Letters*, 1998, **73**, 3046

[67] M. Akiyama, C.-N. Xu, M. Taira, K. Nonaka, T. Watanabe, *Philosophical Magazine Letters*, 1999, **79**, 735

[68] A. Yu, D. Zhang, Y. Hu, R. Yang, *Journal of Materials Science: Materials in Electronics*, 2014, **25**, 4434

[69] H. H. Shin, J. H. Kim, B. Y. Han, J. S. Yoo, *Japanese Journal of Applied Physics*, 2008, **47**, 3524

[70] P. Zhang, M. Xu, Z. Zheng, B. Sun, Y. Zhang, Materials Science and Engineering: B, 2007, **136**, 159

[71] P. Zhang, L. Li, M. Xu, L. Liu, *Journal of Alloys and Compounds*, 2008, **456**, 216

[72] P. Zhang, L. Lingxia, T. Yuming, *Physica B*, 2009, **404**, 4286

[73] Ch. Yuesheng; Z. Ping, Z. Zhentai, *Physica B*, 2008, **403**, 4120

[74] P. Huang, C. Cui, S. Wang, *Optical Materials*, 2009, **32**, 184

[75]   T.Zhou, Z. Song, L.Bian, Q.Ren, Q.Liu *Journal of Rare   Earths,*
       2012, **30,** 632
[76]   D. Si, B.Geng, S. Wang   *CrystEngCommunity* 2010, **12**,
       2722
[77]   P.Huang, Q.Zhang, C. Cui, J. Li, *Optical Materials,* 2011,   **33,** 1252
[78]   J. Zhang, X. Zhang, J.Shi, M.Gong, *Journal of   Luminescence,* 2011,
       131, 2463